Analysis of the Effects of a Resistively Coated Upper Dielectric Layer on the Propagation Characteristics of Hybrid Modes in a Waveguide-Shielded Microstrip Using the Method of Lines

Shyh-Jong Chung, *Member, IEEE,* and Lin-Kun Wu, *Member, IEEE*

Abstract—**In this paper, propagation characteristics of even-symmetric hybrid modes in a waveguide-shielded microstrip in the presence of a resistively coated dielectric layer affixed to the top cover of the housing is analyzed with the method of lines. The resistive boundary condition is employed to model the resistive film. A shielded microstrip line having a unity strip-width-to-substrate-thickness ratio (i.e., $w/h_1 = 1$) placed on top of a 0.635-mm-thick alumina substrate is considered. Based on a $10h_1 \times 7h_1$ reference housing, four different housing arrangements are obtained by varying the structural parameters of the resistively coated dielectric layer. Results obtained indicate that the effects of both the housing walls and the resistively coated upper dielectric layer on the dominant (quasi-TEM) mode are insignificant and may be ignored when frequency is above 15 GHz. For the higher order modes, resistive film appears to be transparent when film resistance is greater than about 1 kΩ, it behaves as a good conductor when film resistance is much smaller than 100 Ω, and in between it results in nonlinear (and even oscillatory) higher order modal behaviors. Apparently, due to the increasing field concentration inside the upper dielectric (as suggested by the increasing ε_{reff}) for a given mode, both the maximum attenuation and the film resistance needed to achieve it increase with frequency and dielectric constant of the upper dielectric layer.**

I. Introduction

MICROSTRIPS are open structures that tend to radiate as the operating frequency increases. However, in practice, hybrid and monolithic microwave and millimeter-wave integrated circuits are enclosed in a metal package to protect the circuit from the environment and to provide electrical isolation between different parts of the subsystem. When an electrically small enclosure is used, a broader single-mode (i.e., quasi-TEM) operating frequency range is obtained. However, approaching package walls results in more field to be present in the air region of the shielded microstrip circuit which modifies the dominant microstrip mode characteristics of uniform lines and discontinuities [1]–[4].

Proximity effects on the dominant mode characteristic can be minimized by the use of an electrically large enclosure which, however, can support several modes. When the frequency approaches or is above the cutoff frequency for higher order mode propagation, erratic circuit behaviors in the form of package resonance or enhanced parasitic coupling among circuit elements have been reported in [2] and [5]–[8]. As was pointed out in [2], shielding effects due to the onset of higher order modes are more important than shielding effects due to wall proximity. This observation is particularly important in view of the constantly increasing circuit complexity and operating frequency in the development of MIC's [9], [10]. As a consequence, aside from being able to predict the shielding effects of the higher order modes, it is perhaps even more desirable and important to devise efficient ways for suppressing them.

Recently, a less expensive and more reliable alternative to the conventional methods for the suppression of package resonances (a summary of these traditional methods can be found in [11]) was proposed [12]. In this latter approach, a dielectric layer coated with a resistive film is fixed under the lid of a package containing a large (M)MIC, using the same processes of fixing the microstrip circuit to the bottom of the package. Since the field associated with the dominant (quasi-TEM) mode is confined mainly in the immediate surroundings of the strip conductor, it would not interact strongly with,

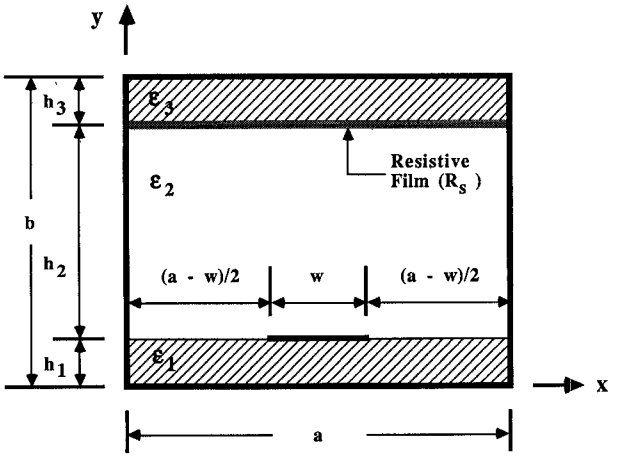

Fig. 1. Cross-sectional view of the waveguide-shielded uniform microstrip line with a resistively coated dielectric layer affixed to the top cover.

Manuscript received May 4, 1992; revised January 22, 1993. This work was supported by the National Science Council of the Republic of China under Grant NSC 81-0404-E-009-529.

The authors are with the Institute of Communication Engineering, National Chiao Tung University, 1001 Ta Hsueh Rd, Hsinchu, Taiwan 30050.

IEEE Log Number 9210204.

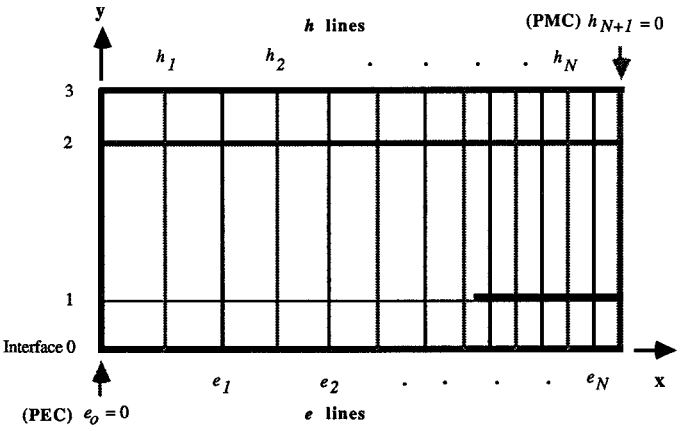

Fig. 2. Illustration of lines used in the nonequidistant discretization scheme over the half of the shielded microstrip structure to be analyzed.

and is thus not attenuated much by, the resistive film. On the other hand, higher order modes, with their fields spread over the entire cross section of the package, will in general experience some loss due to the current flow on the surface of the resistive coating. Package resonance and parasitic coupling among circuit elements may then be suppressed.

While damping performance of a resistively coated dielectric layer on the lowest order box mode of a rectangular cavity was considered in [12], the frequency-dependent complex propagation constants of shielded microstrips modes in a waveguide-type of housing, which includes a resistively coated dielectric layer affixed to its top cover, are analyzed in this paper. A cross-sectional view of the structure to be analyzed is shown in Fig. 1. The method of lines [13], which is available to us for other applications, is used in this analysis. For simplicity, we consider only the cases where the strip conductor is placed symmetrically with respect to the two sidewalls. Furthermore, since the dominant quasi-TEM mode is even-symmetric with respect to the plane of symmetry at $x = a/2$, and for the purpose of demonstrating the efficacy of the resistively coated dielectric layer for attenuating higher order modes, only the even modes that are characterized by having a zero tangential magnetic field at the plane of symmetry are considered in this paper. The odd mode behavior can be analyzed in a similar fashion by replacing the magnetic wall at $x = a/2$ with a corresponding electric wall.

The present method differs from the method of lines documented in [13] in the use of Senior's resistive boundary condition [14] to account for the presence of the resistive film. Therefore, only the major steps used in the traditional method of lines together with the additional resistive boundary algorithm are summarized in Section. II. Some numerical examples obtained for four different housing arrangements are then presented in Section III. Conclusions are presented in Section IV.

II. Formulation

A cross-sectional view of the structure to be analyzed is shown in Fig. 1. For the shielded microstrip considered here, the structure is assumed to be symmetrical along the x-axis and extends uniformly to infinity along the z direction, which thus reduces the problem to a two-dimensional one. For the even modes characteristics to be considered in this paper, the problem space can be halved by introducing a magnetic wall at the plane of $x = a/2$. The resultant structure is shown in Fig. 2, with discretization lines along the y-axis for the z components of the electric and magnetic fields, e_z and h_z. Similarly, an electric wall can be placed at $x = a/2$ for determining the odd-mode characteristics.

Following the procedures described in [13], a transformation procedure is obtained

$$\begin{bmatrix} \underline{E}_m \\ \underline{H}_m \end{bmatrix} = \begin{bmatrix} \underline{V}_m & \underline{Z}_m \\ \underline{Y}_m & \underline{V}_m \end{bmatrix} \begin{bmatrix} \underline{E}_{m-1} \\ \underline{H}_{m-1} \end{bmatrix}, \qquad m = 1,2,3 \quad (1)$$

where, for $p = 0,1,2,3$,

$$\underline{H}_p = \eta_0 \begin{bmatrix} -j\underline{H}_{zp} \\ \underline{H}_{xp} \end{bmatrix} \quad (2a)$$

and

$$\underline{E}_p = \begin{bmatrix} \underline{E}_{xp} \\ -j\underline{E}_{zp} \end{bmatrix} \quad (2b)$$

are the transformed tangential fields at the upper ($p = m$) and lower ($p = m-1$) interface planes of the mth dielectric layer shown in Fig. 2, and $\underline{V}$, $\underline{Y}$, and $\underline{Z}$ are matrices determined by the properties of the layer involved.

After applying the boundary conditions at the perfect electric conductors present at interface 0 and 3 (i.e., $\underline{E}_0 = \underline{E}_3 = 0$), use of (1) yields

$$\underline{H}_{1-} = \underline{Y}_t^{(1)} \underline{E}_1 \quad (3)$$

and

$$\underline{H}_{2+} = -\underline{Y}_t^{(3)} \underline{E}_2 \quad (4)$$

with

$$\underline{Y}_t^{(m)} = \underline{V}_m \underline{Z}_m^{-1}, \qquad m = 1 \text{ or } 3 \quad (5)$$

where sub-superscripts "+" and "−" signify, respectively, that $\underline{H}_m$'s are taken "above" and "below" the corresponding mth interface.

Next, the resistive film at interface 2 is assumed to be characterized by having a finite conductivity σ and a thickness

TABLE I
SUMMARY OF THE ADDITIONAL STRUCTURAL PARAMETERS USED FOR EACH OF THE FOUR HOUSINGS EXAMINED IN THIS PAPER

	h_3/h_1	b/h_1	$\varepsilon_3/\varepsilon_o$	R_s
WA	1	7	9.7	$(0,\infty)$
WB	1	7	1	∞
WC	0	6	N/A	∞
WD	1	7	2.2	$(0,\infty)$

τ which is much smaller than the skin depth, such that it may be modeled as an infinitesimally thin resistive film with a constant surface resistance $R_s = (1/\sigma\tau)\ \Omega$ [14]. It is noted that the resistive film becomes an infinitesimally thin perfect electric conductor when $R_s = 0\ \Omega$, and it is nonexistent when R_s becomes infinite. When crossing such a resistive sheet, the tangential electric fields are continuous while the corresponding tangential magnetic fields are discontinuous, and the two sets of tangential field components must satisfy the following resistive boundary condition [14]:

$$\hat{n} \times \boldsymbol{E}_2 = \boldsymbol{R}_s \hat{n} \times (\boldsymbol{H}_{2+} - \boldsymbol{H}_{2-}) \tag{6}$$

or, in the transform domain,

$$\underline{\boldsymbol{E}}_2 = \frac{\boldsymbol{R}_s}{j\eta_o} (\underline{\boldsymbol{H}}_{2-} - \underline{\boldsymbol{H}}_{2+}) . \tag{7}$$

Then from (4) and (7) we get

$$\underline{\boldsymbol{H}}_{2-} = -\underline{\boldsymbol{Y}}_t^{(3)'} \underline{\boldsymbol{E}}_2 \tag{8}$$

with

$$\underline{\boldsymbol{Y}}_t^{(3)'} = \underline{\boldsymbol{Y}}_t^{(3)} - \frac{j\eta_0}{\boldsymbol{R}_s} . \tag{9}$$

Finally, by substituting (8) into (1), the following relationship is obtained:

$$\underline{\boldsymbol{H}}_{1+} = -\underline{\boldsymbol{Y}}_t^{(2)} \underline{\boldsymbol{E}}_1 \tag{10}$$

where

$$\underline{\boldsymbol{Y}}_t^{(2)} = (\underline{\boldsymbol{Y}}_2 + \underline{\boldsymbol{V}}_2 \underline{\boldsymbol{Y}}_t^{(3)'})(\underline{\boldsymbol{V}}_2 + \underline{\boldsymbol{Z}}_2 \underline{\boldsymbol{Y}}_t^{(3)'})^{-1} . \tag{11}$$

From (3), (10), and the boundary condition at interface 1, an inhomogeneous matrix equation is obtained

$$\underline{\boldsymbol{Z}}\, \underline{\boldsymbol{J}}_1 = \underline{\boldsymbol{E}}_1 \tag{12}$$

where $\underline{\boldsymbol{J}}_1$ represents the transformed current distribution along interface 1. By transforming back to the spatial domain, and recognizing that nonzero conduction currents and zero tengential electric fields exist over the strip portion of the interface 1, a reduced matrix equation can be obtained

$$\boldsymbol{Z}^r \boldsymbol{J}_1^r = 0 \tag{13}$$

where the current vector

$$\boldsymbol{J}_1^r = \begin{bmatrix} j\boldsymbol{J}_x \\ \boldsymbol{J}_z \end{bmatrix} \tag{14}$$

contains only nonzero $\boldsymbol{J}_x$ and $\boldsymbol{J}_z$ over the strip [13]. The desired modal dispersion characteristics of the structure can then be obtained by simply enforcing the condition of $\det\{\boldsymbol{Z}^r\} = 0$.

III. RESULTS AND DISCUSSIONS

Results to be presented in this section are all derived using the following nonequidistant discretization scheme [15]. For the discretization scheme shown in Fig. 2, e_z and h_z are set to zero for the respective e_z-line along the electric wall at $x = 0$, and the h_z-line along the magnetic wall at $x = a/2$. Among the total of Ne_z-line and Nh_z-line used, N_w e_z-line and $N_w - 1$ h_z-line are placed across the strip with a constant subinterval between any two adjacent e_z- and h_z-lines. For lines between the strip edge and the sidewall, this subinterval increases as a geometrical series with quotient q of successive subintervals being a constant [15]. Furthermore, the edge condition is satisfied by positioning the edge of the infinitely long strip half-way between the two adjacent e_z- and h_z-lines [13].

In this paper, four different housing arrangements are used. For convenience, they are designated as housing WA, WB, WC, and WD. For the structural geometry shown in Fig. 1, the following common parameters are used in these housings: $w = h_1 = 0.635$ mm, $\varepsilon_1 = 9.7\varepsilon_o$ (i.e., alumina substrate), $\varepsilon_2 = \varepsilon_o, h_2 = 5h_1$, and $a = 10h_1$. Additional structural parameters are summarized in Table I. It is noted that with a's and b's chosen here, the dominant (quasi-TEM) mode is expected to experience only a minimal degree of proximity effect at lower frequencies within housings WB and WC [4]. Therefore, additional structural parameters associated with housings WA and WD will be used to demonstrate the effects of resistively coated dielectric substrate on the propagation characteristics of higher order modes.

A. Shielded Microstrip with Single Dielectric Substrate

As a numerical check, Fig. 3 compares the dominant mode dispersion curves calculated for: 1) the shielded microstrip contained in housing WB using two discretization schemes with the present method, and 2) the corresponding unshielded microstrip using the closed-form expressions given in [16] (which are considered to be very accurate for unshielded microstrips). Excellent convergence has been achieved in the present method as the results obtained by the two discretization schemes having ($N_w = 15$, $N = 32$, and $q = 1.1$) and ($N_w = 30$, $N = 51$, and $q = 1.1$) are almost identical throughout the entire frequency range. Although not shown here, this also holds when $q = 1$ and 1.2 are used with the ($N_w = 15$, $N = 32$) discretization scheme. Given these, the discretization scheme with ($N_w = 15$, $N = 32$, and $q = 1.1$) is used to obtain the results to be presented in the following. Furthermore, Fig. 3 shows that while all three sets of data are almost identical for frequency above 15 GHz, smaller ε_{reff}

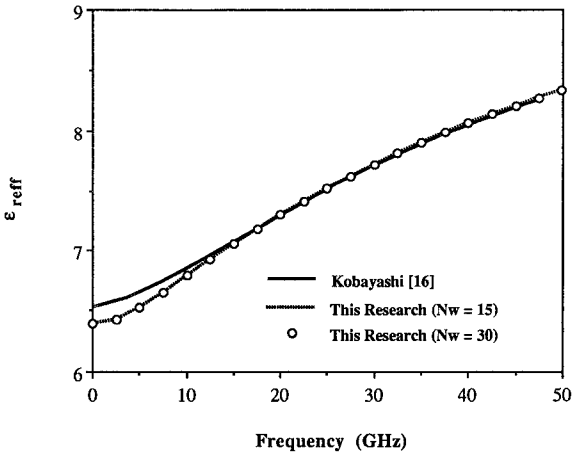

Fig. 3. Comparison of the effective dielectric constant of the dominant mode versus frequency calculated for: 1) the shielded case with housing WB using the present method, and 2) the unshielded case using the closed-form formula of [16]. Two discretization schemes with ($N_w = 15, N = 32, q = 1.1$) and ($N_w = 30, N = 51, q = 1.1$) are used in the present method.

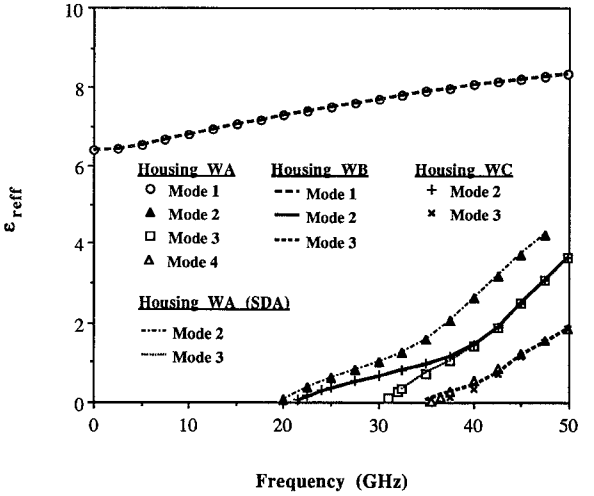

Fig. 4. Effective dielectric constant versus frequency calculated for housings WA (with infinite R_s), WB, and WC by the present method ($N_w = 15, N = 32$, and $q = 1.1$). Data obtained by the spectral-domain approach (SDA) for Modes 2 and 3 of housing WA are also shown for comparison.

are predicted by the present method for the shielded case at lower frequencies; similar observations were also made in [17] for the case of a waveguide-shielded microstrip having finite metallization thickness. In summary, Fig. 3 reveals that: 1) convergent and accurate results can be obtained by the present method, and 2) proximity effect of the approaching walls on the dominant mode dispersion characteristics can be ignored for frequency above 15 GHz.

B. Shielded Microstrip with Additional Upper Dielectric Layer

Next, effects of the additional upper dielectric layer (with infinite R_s) on the modal dispersion behaviors are illustrated in Fig. 4 for housings WA and WB. Fig. 4 also shows the dispersion data obtained by the spectral-domain approach (SDA) for Modes 2 and 3 of housing WA, which clearly demonstrates the accuracy of the present method in analyzing higher order modal behaviors. In addition, for future reference purposes, dispersion curves for the first two higher order modes (i.e., Modes 2 and 3) associated with housing WC are also illustrated in Fig. 4.

As can be seen, for housings WA and WB, dominant mode (i.e., Mode 1) dispersion curves are almost the same. This should be expected since the dominant modal fields concentrate mainly near the strip conductor such that the effect due to the additional upper dielectric layer in housing WA is insignificant. On the other hand, since higher order modal fields (i.e., Modes 2, 3, etc.) extend over the entire cross section of the housing, modal structures are modified by the presence of the upper (non-air) dielectric layer. Specifically, for the results to be discussed next, it is noted that below about 35 GHz, two propagating higher order modes are supported by housing WA (and WD, for which the dispersion curves are not shown here to prevent further cluttering the drawing) and only one each in housings WB and WC (which, in the absence of the upper dielectric, have quite similar modal dispersion behaviors). In the following, the influences of the resistive

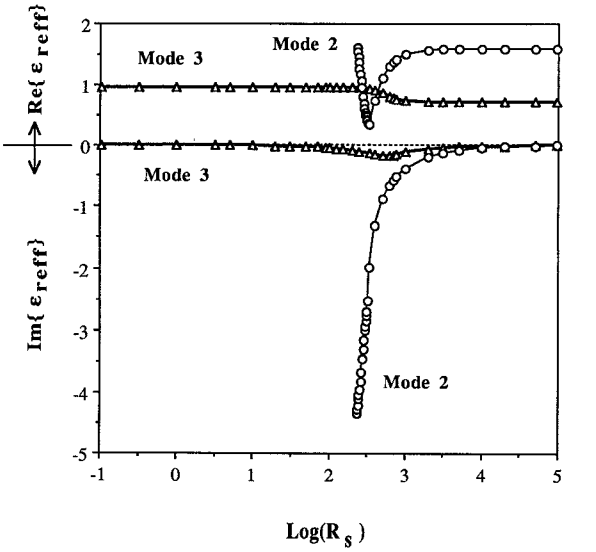

Fig. 5. Complex effective dielectric constant versus $\log(R_s)$ calculated for Modes 2 and 3 of housing WA. (Frequency = 35 GHz, $N_w, = 15, N = 32$, and $q = 1.1$.)

coating on the modal dispersion behaviors of Modes 2 and 3 of housing WA will be investigated further.

C. Shielded Microstrip with a Resistively Coated Upper Dielectric Layer

Fig. 5 displays the variations of the complex ε_{reff} versus $\log(R_s)$ for Modes 2 and 3 of housing WA at 35 GHz; the complex ε_{reff} for which $\det\{Z^r\} = 0$ is satisfied is determined using the Muller's method, where ε_{reff} found for a given R_s is used as the initial guess for the next R_s when R_s decreases from infinity to zero. Although not shown here, the real part of ε_{reff} of the dominant mode remains essentially the same as shown in Fig. 4, while only negligibly small values of the imaginary part of ε_{reff} (and attenuation constant) are detected, for all resistance values considered.

For Mode 3, when $\log(R_s) > 3.5$, the effects of the film are rather insignificant such that $\mathrm{Re}\{\varepsilon_{reff}\}$ assumes essentially the same value as that shown in Fig. 4 (i.e., infinite R_s) while $\mathrm{Im}\{\varepsilon_{reff}\} \approx 0$. However, when $\log(R_s) < 1.5$, Mode 3 of housing WA has an $\mathrm{Re}\{\varepsilon_{reff}\} \approx 0.967$ (and $\mathrm{Im}\{\varepsilon_{reff}\} \approx 0$), which is the same as that of the Mode 2 of housing WC shown in Fig. 4. When $\log(R_s)$ decreases from 3.5 to 1.5, the magnitude of $\mathrm{Im}\{\varepsilon_{reff}\}$ increases first, and reaches its maximum value when $\log(R_s) \approx 2.7$ (i.e., $R_s \approx 500\ \Omega$) before decreasing again to zero. These observations indicate that Mode 3 of housing WA reduces to the propagating Mode 2 of housing WC as zero R_s is approached.

In contrast to Mode 3, computations are made only for $\log(R_s) > 2.373$ (i.e., $R_s > 236\ \Omega$) for Mode 2. Since the zero and pole of $\det[Z^r]$ are so close to each other, an accurate determination of the zero for Mode 2 becomes extremely difficult when $\log(R_s) < 2.54$. This is reflected by the fact that for the data shown in Fig. 5, computations are actually performed for more than 1000 R_s values (each requiring a number of iterative steps) over the range of $2.54 > \log(R_s) > 2.373$ (i.e., $350\ \Omega > R_s > 236\ \Omega$)! Due to this numerical difficulty, we are not able to proceed computation any further. For the data obtained and shown in Fig. 5, it is found that both $\mathrm{Re}\{\varepsilon_{reff}\}$ and $\mathrm{Im}\{\varepsilon_{reff}\}$ of Mode 2 remain fairly constant for large value of R_s. When $\log(R_s)$ decreases below 3 (i.e., $R_s < 1\ k\Omega$), magnitude of the $\mathrm{Im}\{\varepsilon_{reff}\}$ increases monotonically while $\mathrm{Re}\{\varepsilon_{reff}\}$ drops rapidly before reaching a minimum value of 0.353, when $\log(R_s) = 2.54$ (i.e., $R_s = 350\ \Omega$), it increases afterward. In terms of complex propagation constant, the phase exhibits similar oscillatory behavior as $\mathrm{Re}\{\varepsilon_{reff}\}$ while attenuation constant shows the same monotonic behavior as $\mathrm{Im}\{\varepsilon_{\mathrm{reff}}\}$. When computation was finally terminated at $\log(R_s) = 2.373$, the attenuation constant has reached an extremely large value of 78.4 dB/cm. For comparison, the maximum attenuation suffered by Mode 3 is only about 6 dB/cm at $\log(R_s) \approx 3$ [see Fig. 7(b)].

The above data indicate that resistive film appears to be transparent to the modal fields when $R_s > 1\ k\Omega$, it is quite lossy (mainly due to absorption) for R_s in the 100's Ω range, and it behaves as a good conductor when $R_s \ll 100\ \Omega$. To examine why Mode 2 suffers more attenuation than Mode 3, magnitudes of the total tangential electric field ($|E_{\tan}|$ in arbitrary unit) computed for Modes 2 and 3 along interfaces 1 ($y = h_1$) and 2 ($y = h_1 + h_2$) of housing WA with infinite R_s are shown in Figs. 6(a) and (b), respectively. It is noted that since normalization of the field strength over different modes is difficult, ratio of the field strength obtained at the two interfaces for each mode is used to infer the loss mechanism.

Figs. 6(a) and (b) reveals that Mode 2 has a much larger ratio of the (average) field strength along interface 2 to that of interface 1 than Mode 3. Since $|E_{\tan}|$ has to vanish at the top wall, the above comparison also points out that Mode 2 has a larger portion of its energy distributed in the upper dielectric region. As a consequence, Mode 2 has a higher ε_{reff} than Mode 3 when the resistive film is absent (see Fig. 4) and, more importantly, it shall lose more energy (by means of absorption) to the resistive film (see Fig. 5). The generally smaller and relatively uniform field distribution found along

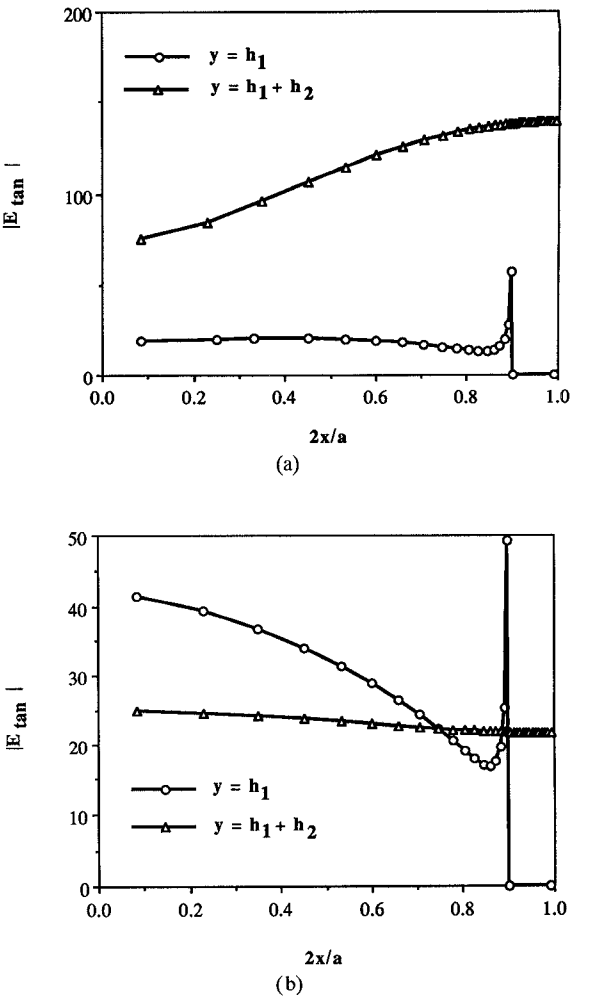

Fig. 6. Distributions of the magnitude of the total tangential electric fields along interfaces 1 and 2 for: (a) Mode 2, and (b) Mode 3 of housing WA with infinite R_s. (Frequency = 35 GHz, $N_w = 15, N = 32$, and $q = 1.1$.)

interface 2 for Mode 3 indicates that only a small amount of its energy is distributed inside the upper dielectric (at 35 GHz). This should also explain why, as shown in Fig. 4, its ε_{reff} is so similar to that of the Mode 2 of housing WB which has no upper dielectric.

In Figs. 7(a) and (b), variations of the real and imaginary parts of the propagation constant k_z (i.e., $k_z = \beta - j\alpha = (\sqrt{\varepsilon_{reff}}\, k_o)$ as a function of $\log(R_s)$ are depicted for: 1) Mode 2 at 25 GHz, 2) Mode 2 at 30 GHz, and 3) Mode 3 at 35 GHz. Since attenuation constant for Mode 2 at 35 GHz reaches a very large value of 78 dB/cm when computation was terminated at $\log(R_s) = 2.373$, it is not displayed here for clarity. Fig. 7(a) shows that the effects of the resistive film on β's are insignificant in all three cases considered when $\log(R_s)$ is greater than 3 (i.e., $R_s > 1\ k\Omega$). This is followed by a transition region over a range of $3 > \log(R_s) > 1.5$ in which decreasing β's are observed. As zero R_s is approached, β's obtained for the Mode 2 of housing WA at 25 GHz and 30 GHz and Mode 3 at 35 GHz reduce, respectively, to that of the Mode 2 in housing WC (specifically, from ε_{reff} data shown in Fig. 4, we have: $\varepsilon_{reff} = 0.373$, or $\beta = 3.196$ rad/cm, at 25 GHz; $\varepsilon_{reff} = 0.683$,

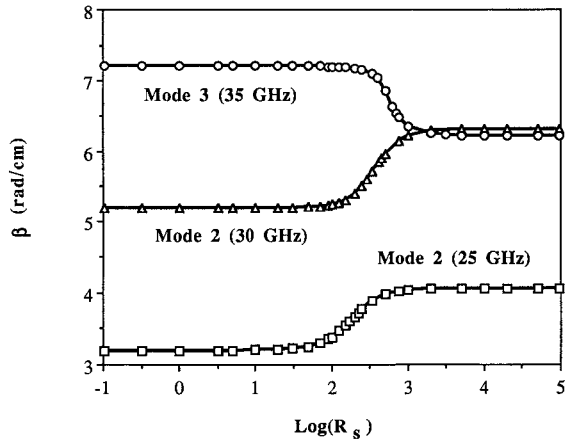

(a)

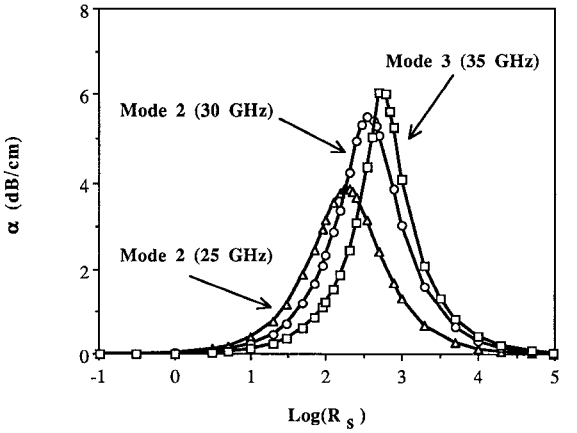

(b)

Fig. 7. (a) Phase constant and (b) attenuation constant versus $\log(R_s)$ calculated for Mode 2 at 25 and 30 GHz, and Mode 3 at 35 GHz, of housing WA. ($N_w = 15, N = 32$, and $q = 1.1$.)

or $\beta = 5.192$ rad/cm, at 30 GHz; and $\varepsilon_{reff} = 0.967$, or $\beta = 7.207$ rad/cm, at 35 GHz). These results indicate that hybrid mode dispersion behavior inside housing WC can be recovered from that of the housing WA with diminishing (but nonzero) film resistance. This may thus be viewed as a validity check on the accuracy of the higher order mode data (in particular, the effects of the resistive film) obtained by the present method.

Similar to the behavior of $\mathrm{Im}\{\varepsilon_{reff}\}$ shown in Fig. 5 for Mode 3 at 35 GHz, all three sets of data shown in Fig. 7(b) reveal that α's increase first as $\log(R_s)$ decreases from 5, and a maximum value is reached in each case before decreasing again as $\log(R_s)$ decreases further. Furthermore, comparison between the maximum attenuations suffered by the Mode 2 at 25 and 30 GHz indicates, that the maximum attenuation, and the film resistance needed to achieve it, increases with increasing frequency. As suggested by the increasing ε_{reff} found in Fig. 4, this again attributed to the increasing field/energy distribution inside the upper dielectric layer as frequency increases.

Finally, the effect of the material used for the upper layer is demonstrated in Fig. 8. In this case, α versus $\log(R_s)$, calculated at 30 GHz for the Mode 2 of housing WD, is

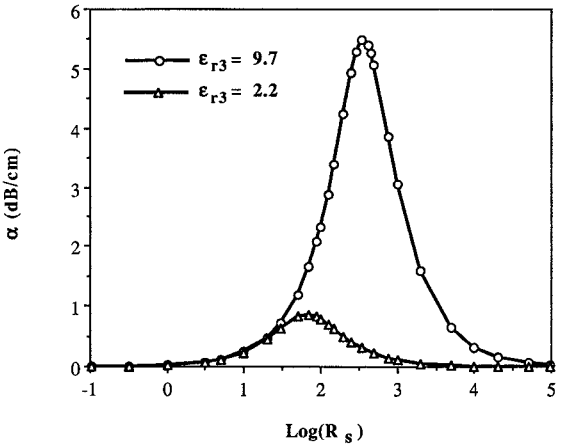

Fig. 8. Attenuation constant versus $\log(R_s)$ calculated for Mode 2 of housings WA (i.e., $\varepsilon_{r3} = 9.7$) and WD (i.e., $\varepsilon_{r3} = 2.2$). (Frequency = 30 GHz, $N_w = 15, N = 32$, and $q = 1.1$.)

compared to the corresponding data obtained for the Mode 2 of housing WA. As shown in Table I, the only difference between the two is that $\varepsilon_3 = 9.7\varepsilon_o$ and $2.2\varepsilon_o$ are used with housings WA and WD, respectively. With the remaining structural parameters being the same, smaller ε_3 used in housing WD apparently results in weaker field strength inside its upper dielectric layer. As a consequence, Fig. 8 shows the smaller attenuation constants are obtained for housing WD.

IV. Conclusions

In this paper, use of a resistively coated dielectric layer affixed to the top wall of the housing for the suppression of higher order shielded microstrip modes is investigated. For simplicity, only even modes are considered; nonetheless, the formulation presented in this paper can be extended to the analysis of odd-mode characteristics simply by replacing the magnetic wall used here with the corresponding electric wall.

It is found that for the specific housings considered, proximity effects of the housing walls on the dominant mode characteristics may be ignored for frequency exceeding 15 GHz. Since the dominant modal fields concentrate mainly in the immediate surroundings of the strip conductor, the above statement holds both with and without the presence of the resistively coated dielectric layer. On the other hand, as higher order modal fields extend over the entire cross section of the housing, interactions with the coated upper dielectric layer are expected.

For large R_s (i.e., greater than about 1 $k\Omega$), film is almost transparent to the modal fields such that β remains essentially the same as, while α increases only slightly from, the case of infinite R_s. For R_s in the order of 100's of ohms, film becomes absorptive, and significant interaction between the crossing fields and the film occurs. Nonlinear, and even oscillatory, modal propagation characteristics are found as R_s varies in this range. In general, except for the oscillatory behavior found in Mode 2 of housing WA at 35 GHz, β shifts monotonically toward that of the case of zero R_s; it stays at that value when R_s continues to decrease toward 0 Ω. On the other hand, α continues to increase until a maximum value is reached, and

then decreases to zero when R_s approaches zero. For a given mode (e.g., Mode 2 of housings WA and WD), ε_{reff} increases as frequency and/or dielectric constant of the material used in the upper layer increases. It may serve as an indication of increasing field concentration inside the upper dielectric. As such, the maximum attenuation, and film resistance needed to achieve it, increase with frequency and dielectric constant of the upper dielectric layer. For $R_s \ll 100\ \Omega$, film behaves as a good conductor with low conductor loss.

Finally, Mode 2 (at 25 and 30 GHz) and Mode 3 (at 35 GHz) of housing WA are found to transform smoothly to the corresponding Mode 2 of housing WC as film resistance decreases from infinity toward (but never reached) zero. Since the modal characteristics associated with housing WC (see Fig. 4) are obtained in the absence of the resistively coated upper dielectric layer, these results may be considered as an independent check on the validity of the use of the present method for the determination of the effects of the resistively coated dielectric layer on the hybrid modal behaviors.

ACKNOWLEDGMENT

The authors are grateful to the reviewers for their critical comments which improved this paper.

REFERENCES

[1] L. P. Dunleavy and P. B. Katehi, "A generalized method for analyzing shielded thin microstrip discontinuities," *IEEE Trans. Microwave Theory Tech.*, vol. 36, pp. 1758–1766, Dec. 1988.

[2] ——, "Shielding effects in microstrip discontinuities," *IEEE Trans. Microwave Theory Tech.*, vol. 36, pp. 1767–1773, Dec. 1988.

[3] S. March, "Microstrip packaging: Watch the last step," *MIcrowaves*, pp. 83–94, Dec. 1981.

[4] L. K. Wu and Y. C. Chang, "Characterization of the shielding effects on the frequency-dependent effective dielectric constant of a waveguide-shielded microstrip using the finite-difference time-domain method," *IEEE Trans. Microwave Theory Tech.*, vol. 39, pp. 1688–1693, Oct. 1991.

[5] R. H. Jansen and L. Wiemer, "Full-wave theory based development of mm-wave circuit models for microstrip open end, gap, step, and tee," in *IEEE MTT-S Int. Microwave Symp. Dig.*, 1989, p. 779–782.

[6] A. Hill and V. K. Tripathi, "An efficient algorithm for the three-dimensional analysis of passive microstrip components and discontinuities for microwave and millimeter-wave integrated circuits," *IEEE Trans. Microwave Theory Tech.*, vol. 39, pp. 83–91, Jan. 1991.

[7] A. Sabban and K. C. Gupta, "Effects of packages on parasitic coupling among microstrip discontinuities in MMICs," *Int. J. Microwave Millimeter-Wave Computer-Aided Eng.*, vol. 1, no. 4, pp. 403–410, 1991.

[8] J. Moore and H. Ling, "Characterization of a 90° microstrip bend with arbitrary miter via the time-domain finite difference method," *IEEE Trans. Microwave Theory Tech.*, vol. 38, pp. 405–410, Apr. 1990.

[9] Special issue on Multifunctions MMIC's and Their System Applications, *IEEE Trans. Microwave Theory Tech.*, vol. 38, Sept. 1990.

[10] Special section on RF Integrated Electronics, *Proc. IEEE*, vol. 79, Mar. 1991.

[11] R. K. Hoffman, *Handbook of Microwave Integrated Circuits.* Norwood, MA: Artech House, 1987, pp. 399–400.

[12] D. F. Williams, "Damping of the resonant modes of a rectangular metal package," *IEEE Trans. Mcrowave Theory Tech.*, vol. 37, pp. 253–256, Jan. 1989.

[13] R. Pregla and W. Pascher, "The method of lines," in *Numerical Techniques for Microwave and Millimeter-Wave Passive Structures*, T. Itoh, Ed. New York: Wiley, 1989, ch. 6.

[14] T. B. A. Senior, "Approximate boundary conditions," *IEEE Trans. Antennas Propagat.*, vol. 29, pp. 826–829, Sept. 1981.

[15] H. Diestel and S. B. Worm, "Analysis of hybrid field problems by the method of lines with nonequidistant discretization," *IEEE Trans. Microwave Theory Tech.*, vol. 32, pp. 633–638, June 1984.

[16] M. Kobayashi, "A dispersion formula satisfying recent requirements in microstrip CAD," *IEEE Trans. Microwave Theory Tech.*, vol. 36, pp. 1246–1250, Aug. 1988.

[17] F. J. Schmuckle and R. Pregla, "The method of lines for the analysis of planar waveguides with finite metallization thickness," *IEEE Trans. Microwave Theory Tech.*, vol. 39, pp. 107–111, Jan. 1991

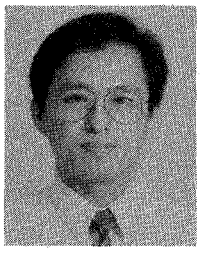

Shyh-Jong Chung (M'92) was born in Taipei, Taiwan, Republic of China, on January 18, 1962. He received the B.S.E.E. degree in 1984, and the Ph.D. degree in 1988, both from National Taiwan University, Taipei, Taiwan.

Since 1988, he has been with the Department of Communication Engineering, National Chiao Tung University, Hsinchu, Taiwan, R.O.C., where he is currently an Associate Professor. His areas of interests include waveguide discontinuities, EMI, wave propagation, and numerical techniques in electromagnetics.